eNeuro

Research Article: New Research | Disorders of the Nervous System

Synaptic integration in CA1 pyramidal neurons is intact despite deficits in GABAergic transmission in the *Scn1a* haploinsufficiency mouse model of Dravet syndrome

https://doi.org/10.1523/ENEURO.0080-22.2022

Cite as: eNeuro 2022; 10.1523/ENEURO.0080-22.2022

Received: 21 February 2022
Revised: 29 March 2022
Accepted: 27 April 2022

Title: Synaptic integration in CA1 pyramidal neurons is intact despite deficits in GABAergic transmission in the *Scn1a* haploinsufficiency mouse model of Dravet syndrome

Abbreviated Title: Synaptic physiology in *Scn1a* Het hippocampus

Authors: Jessica Hotard Chancey and MacKenzie Allen Howard
Department of Neurology, Dell Medical School, Austin, TX; Department of Neuroscience and Center for Learning and Memory, University of Texas at Austin, Austin, TX

Author Contributions: JHC designed and performed experiments, analyzed data, and wrote the paper. MH designed experiments and wrote the paper.

Correspondence should be addressed to mackenziehoward@austin.utexas.edu.

Number of figures: 7
Number of tables: 1
Number of words in abstract: 229
Number of words in significance statement: 97
Number of words in introduction:635
Number of words in discussion: 1640

Acknowledgements: This work would not be possible without the generous gift of *Scn1a* transgenic mice from Dr. Jennifer Kearney at Northwestern University. We would like to thank Dr. Audrey Brumback and members of the Howard and Brumback labs for helpful discussions, Dr. Scott Baraban for long-standing mentorship and support, and our technicians who aided in animal care: Mendee Geist; Alexandra Munson; Meredith McCarty; Aurora Weiden; Madelynne Campbell; Joy Adler.

Conflict of Interest: Authors report no conflict of interest.

Funding: Dravet Syndrome Foundation (postdoctoral fellowship to JHC); postdoctoral fellowship to JHC and a Young Investigator Award to MAH from the American Epilepsy

33 Society; NIH/NINDS (R01 NS112500-01); startup funds from Dell Medical School at the
34 University of Texas at Austin

Abstract

Mutations of *SCN1A*, which encodes the voltage-gated sodium channel $Na_V1.1$, can cause epilepsy disorders such as Dravet syndrome that are comorbid with wide-ranging neurological dysfunction. Many studies suggest that $Na_V1.1$ haploinsufficiency causes forebrain GABAergic interneuron hypoexcitability, while pyramidal neuron physiology is mostly unaltered, and that this serves as a primary cell physiology phenotype linking mutation to disease. We hypothesized that deficits in inhibition would alter synaptic integration during activation of the hippocampal microcircuit, thus disrupting cellular information processing and leading to seizures and cognitive deficits. We tested this hypothesis using *ex vivo* whole-cell recordings from CA1 pyramidal neurons in a heterozygous *Scn1a* knockout mouse model and wild type littermates, measuring responses to single and patterned synaptic stimulation and spontaneous synaptic activity. Overall, our experiments reveal a surprising normalcy of excitatory and inhibitory synaptic temporal integration in the hippocampus of *Scn1a* haploinsufficient mice. While miniature IPSCs and feedforward inhibition and were decreased, we did not identify a pattern or frequency of input that caused a failure of synaptic inhibition. We further show that reduced GABA release probability and subsequent reduced short-term depression may act to overcome deficits in inhibition normalizing input/output functions in the *Scn1a* haploinsufficient hippocampus. These experiments show that CA1 pyramidal neuron synaptic processing is surprisingly robust, even during decreased interneuron function, and more complex circuit activity is likely required to reveal altered function in the hippocampal microcircuit.

Significance statement

Mouse models of genetic epilepsy disorders are useful tools for better understanding the neurophysiology underlying the seizures and cognitive comorbidities of disease. Here, we use a *Scn1a* haploinsufficieny model of Dravet syndrome (DS) to investigate synaptic integration and input/output functions, which are fundamental forms of neuronal information processing. We found that while DS model hippocampal pyramidal neurons had modest deficits in inhibition, synaptic integration and input/output functions were surprisingly normal. We also found that changes in GABA release probability may be a compensatory mechanism by which the hippocampal circuit overcomes deficits in inhibition to normalize input/output functions.

Introduction

Disruption of the most vital building blocks of neural signaling lead to the most severe neurological outcomes. The *SCN1A* gene encodes one such foundational component of neuronal excitability, $Na_v1.1$, a voltage-gated sodium channel alpha subunit that supports action potential generation in many neurons (Catterall et al. 2010). Mutations to *SCN1A* lead to epilepsy disorders ranging from simple febrile seizures to the spectrum of generalized epilepsy with febrile seizures plus (GEFS+) disorders (Catterall et al. 2010; Escayg and Goldin 2010). Patients with a mutation that renders one allele of *SCN1A* nonfunctional often present with the most severe form of GEFS+: Dravet syndrome (DS, aka severe myoclonic epilepsy in infancy: SMEI) (Claes et al. 2001; Marini et al. 2011). With limited treatment options, DS is a profoundly devastating

disease characterized by frequent, severe seizures, developmental delays, a range of comorbid neurological and cardiac deficits, and high mortality rates (Dravet 2011).

The epilepsy, comorbidities, and high mortality exhibited by DS patients are recapitulated in genetically engineered animal models of *SCN1A* disruption, including rat (Mashimo et al. 2010), mouse (Mistry et al. 2014; Yu et al. 2006), zebrafish (Baraban et al. 2013), and drosophila (Sun et al. 2012). Initial characterization of heterozygous *Scn1a* mice revealed decreased sodium currents and action potential generation in GABAergic interneurons in cortex and hippocampus, resulting in decreased synaptic inhibition (Yu et al. 2006). In contrast, sodium currents in pyramidal neurons were unaffected. Work in animal models across phyla, in heterozygous knockout and human disease mutation knock-in models, and interneuron specific $Na_v1.1$ knockouts offer support to the hypothesis that decreased inhibitory neuron function is an electrophysiological signature of, and major mechanism underlying, neural dysfunction in *SCN1A*-linked epilepsy disorders (Catterall 2018).

Further studies have added depth and complexity to the interneuron-dysfunction hypothesis of DS. *In vivo* spike rates of interneurons have been recorded to be normal or even elevated during ongoing activity in heterozygous mice (De Stasi et al. 2016; Tran et al. 2020). Further, the decreased intrinsic excitability of parvalbumin- and somatostatin-expressing interneurons is transient, normalizing to wild type levels after a developmental delay (Almog et al. 2021; Favero et al. 2018). This suggests that other developmental abnormalities or compensatory changes in the neural circuitry persist beyond the recovery of function of these inhibitory neurons. A recent study found that while parvalbumin interneurons are hypoexcitable in the dentate gyrus of young adult

Scn1a+/- mice, the magnitude of evoked inhibition was modestly higher, not lower, in dentate granule cells in response to perforant path stimulation, and that excitatory/inhibitory ratio and granule cell recruitment did increase, but due to increases in excitatory input rather than deficits in inhibition (Mattis et al. 2022). Finally, vasoactive intestinal peptide (VIP)-expressing neurons, which largely target other GABAergic interneurons, and therefore disinhibit neural circuitry, also exhibit excitability deficits in heterozygous mice (Goff and Goldberg 2019). Thus, the mechanism underlying DS is more complicated than simple circuit disinhibition due to GABAergic neuron hypoexcitability.

Neural circuit activity and information processing depend on the complex integration of temporally patterned excitatory and inhibitory synaptic inputs (Stuart and Spruston 2015). We hypothesized that deficits in interneuron function would alter synaptic integration and synaptic input/action potential output functions in forebrain pyramidal neurons, serving as a circuit mechanism by which interneuron hypofunction causes cognitive processing deficits of DS. We tested this hypothesis by examining temporal synaptic integration and detailing excitatory and inhibitory synaptic physiology in CA1 hippocampal pyramidal neurons in *ex vivo* slices from *Scn1a* heterozygous and wild type littermate mice. Despite clear evidence of severe epilepsy, broad neurological dysfunction, and early death in the *Scn1a* deficient mouse model used here (Miller et al. 2014; Mistry et al. 2014; Tran et al. 2020), we found only subtle changes to synaptic inhibition, and overall, synaptic integration and input/output functions were relatively unchanged in the hippocampus of this Dravet syndrome model.

Methods

Animals. All procedures were approved by the Institutional Animal Care and Use Committee at our institution. A breeding colony of *Scn1a*$^{+/-}$ mice (a generous gift from Dr. Jennifer Kearney) was maintained on the 129S6/SvEvTac background strain (Taconic). Experimental animals were produced by crossing these mice with wild type (WT) C57Bl/6J mice (Jackson Labs, Strain #000664). All experiments were performed on the 129.*Scn1a*$^{+/-}$ x C56/B6J F1 generation as in Mistry et al. (2014). Experimental animals were male and female 129/C57 *Scn1a*$^{+/-}$ (Het), while male and female wild type 129/C57 *Scn1a*$^{+/+}$ (WT) littermates served as controls. Pups were toe-clipped at ~P7 for identification and tail tissue samples were taken for genotyping by PCR (Miller et al. 2014). All experiments were performed in mice age P21-38 (shaded area in Fig. 1A). A subset of mice were maintained in their homecages and checked on daily for a Kaplan-Meier analysis of survival (Fig. 1A). Of the Het mice monitored (n=25), the first incidence of mortality was recorded on postnatal day (P)17, 50% died by P25, while 24% survived at least 100 days. No WT littermate deaths were recorded (n=30).

Acute slice preparation. Mice were injected intraperitoneally with a mix of ketamine (90 mg/kg) and xylazine (10 mg/kg). Once deep anesthesia was confirmed by lack of response to toe pinch, mice were transcardially perfused with ice-cold, oxygenated cutting solution, containing (in mM): 205 sucrose; 25 sodium bicarbonate; 2.5 KCl; 1.25 sodium phosphate; 7 $MgCl_2$; 7 D-glucose; 3 sodium pyruvate; 1.3 ascorbic acid; 0.5 $CaCl_2$. Perfused brains were removed and hemisected. The midline was placed down and the dorsal portion of the brain was removed using a scalpel blade,

115 angled at ~30º (Poolos and Jones 2004). The cut side was then mounted in the slicing
116 chamber of a Leica VT1200 vibratome. 300 μm horizontal hippocampal slices were
117 made from brains submerged in ice-cold, oxygenated cutting solution. Sections were
118 then incubated for 30 minutes at 37° C, thereafter at room temperature, in holding
119 solution containing (in mM): 125 NaCl; 25 sodium bicarbonate; 2.5 KCl; 1.25 sodium
120 phosphate; 12.5 D-glucose; 2 $MgCl_2$; 2 $CaCl_2$; 1.3 ascorbic acid; 3 sodium pyruvate.
121
122 *Whole-cell electrophysiology*. Slices strictly from the intermediate region of the
123 dorsal-ventral axis of the hippocampus were used, as pyramidal neuron intrinsic
124 excitability, morphology, and synaptic physiology and plasticity all change along this
125 axis (Dougherty et al. 2012; Malik et al. 2016; Milior et al. 2016). Slices were placed in a
126 recording chamber and continuously bathed in warm (32° C), oxygenated artificial
127 cerebrospinal fluid (ACSF), containing (in mM): 125 NaCl, 25 NaHCO3, 2.5 KCl, 1.25
128 NaH2PO4, 1 MgCl2, 2 CaCl2. For some experiments, synaptic receptors were
129 pharmacologically blocked: $GABA_A$ receptors with gabazine (gbz, 10 μM), AMPA
130 receptors with NBQX (10 μM), NMDA receptors with APV (50 μM) in the ACSF. Patch
131 pipettes were pulled to resistances of 3-6 MΩ. Pipettes were filled with either potassium
132 gluconate-based or cesium-based solutions. Potassium gluconate internal contained (in
133 mM): 120 K-gluconate, 20 KCl, 10 HEPES, 4 NaCl, 1 EGTA; 4 Mg-ATP, 0.3 Na-GTP, 7
134 phosphocreatine disodium salt hydrate. Cesium methanesulfonate internal contained (in
135 mM): 120 CsMeS; 4 NaCl; 6 CsCl; 10 HEPES; 1 EGTA; 4 Mg-ATP, 0.3 Na-GTP, 7
136 phosphocreatine disodium salt hydrate; 5 QX-314. Cesium chloride based internal
137 contained (in mM): 80 CsCl; 45 CsMeS; 4 NaCl; 6 CsCl; 10 HEPES; 1 EGTA; 4 Mg-

ATP, 0.3 Na-GTP, 7 phosphocreatine disodium salt hydrate; 5 QX-314. Slices were visualized using a Zeiss Axio Examiner, an infrared digital camera (Zeiss Axiocam 503) and Dodt contrast optics. Neurons with depolarized membrane potential (>-50 mV) or high series resistance (>25 MΩ) were excluded from the study. Synaptic stimulation via activation of the Schaffer collateral axons was performed using a bipolar stimulating electrode (Microprobes) placed in the stratum radiatum near the CA2/CA1 border and a constant current stimulus isolator (World Precision Instruments).

Data were acquired using a MultiClamp 700B amplifier (Molecular Devices) and digitized using an InstruTECH LIH8+8 (HEKA) at a sampling rate of 10 kHz, then filtered at 4 kHz. Data were acquired using Axograph acquisition software. After measuring resting membrane potential in current clamp experiments, a holding current was applied to give all neurons a baseline membrane potential of ~-70 mV. Action potential input/output curves and voltage sag were measured using 250 ms-long depolarizing and hyperpolarizing current steps. Voltage sag was calculated as the peak negative voltage minus the steady state negative voltage just prior to the end of the hyperpolarizing step when cell was hyperpolarized to -90 mV. For synaptic stimulation experiments, threshold stimulus intensity was measured as the lowest stimulus power that consistently produced a measurable response.

Data analysis and statistics. All data are presented as mean ± SEM. Data were analyzed using either Student's t-tests, Mann-Whitney tests, Kolmogorov-Smirnov tests, or repeated measures analysis of variance (RM ANOVA) followed by post hoc Sidak's multiple comparisons tests, as appropriate using GraphPad Prism 7.

Results

Firing properties of CA1 pyramidal neurons are normal in Scn1a Het mice. Previous studies have reported that pyramidal neurons in *Scn1a* haploinsufficiency mouse models have relatively normal intrinsic physiological properties (Almog et al. 2021; Hedrich et al. 2014; Rubinstein et al. 2015), while others have found increased intrinsic excitability (Mistry et al. 2014). Because multiple investigators have independently engineered *Scn1a* transgenic mice, our initial experiments served to establish measures of baseline excitability in CA1 hippocampal pyramidal neurons in this particular line in our hands. Whole-cell current clamp recordings showed that many standard electrophysiological measures were statistically indistinguishable in Het neurons compared with control, including resting membrane potential, input resistance, membrane time constant, capacitance, and voltage sag (Table 1).

Suprathreshold depolarizing current steps were used to evoke and quantify action potential parameters. Like previous reports in other *Scn1a* knockout mouse lines (Almog et al. 2021; Dyment et al. 2020; Hedrich et al. 2014), action potentials were largely unchanged in Het neurons compared to littermate controls. This can be observed in quantification of number of spikes evoked as a function of current injection (Fig. 1B; WT n = 7; Het n = 10; two-way RM ANOVA: main effect of current $p < 0.0001$; main effect of genotype $p = 0.87$; interaction of current and genotype $p = 0.99$). Measures of rheobase, voltage threshold, first spike rise time and half width were also similar across genotypes (Table 1).

184 *Functional integration of excitation and inhibition are unchanged despite*
185 *decrements in inhibition in Scn1a haploinsufficiency.* Our central hypothesis was that
186 decrements in GABAergic interneuron excitability caused by *Scn1a* haploinsufficiency
187 would cause changes in the output of pyramidal neurons in response to activation of the
188 circuit. We tested this hypothesis with *ex vivo* recordings from CA1 pyramidal neurons
189 in current clamp, using a K-gluconate-based internal solution and stimulating the
190 Schaffer collateral (SC) pathway.
191 We hypothesized that inhibitory dysfunction would lead to larger postsynaptic
192 potentials (PSPs) and increased firing rates in Het neurons. To the contrary, we found
193 that PSPs in Het and WT neurons, evoked by a single stimulation of SC axons (Fig.
194 2A), had statistically equivalent peak amplitudes across a broad range of stimulus
195 intensities (Fig. 2B; two-way RM-ANOVA; stimulus intensity: $p < 0.0001$; genotype: $p = 0.44$; intensity X genotype interaction: $p = 0.36$). While the lack of difference between
196
197 genotypes was contrary to our original hypothesis, it is possible that other changes
198 within the circuit such as homeostatic plasticity could compensate for decrements in
199 inhibition. Thus, we repeated this experiment comparing synaptic responses with
200 inhibition blocked with gabazine (gbz; 10 μm) to measure isolated excitatory input. Our
201 expectation was that if excitation was scaled downward in Het neurons, WT neurons
202 would exhibit larger responses than Het when inhibition was blocked. Instead, bath
203 application of gabazine increased the postsynaptic responses of both genotypes
204 equivalently. PSPs amplitude (Fig. 2C; measured as area under the curve with spikes
205 truncated because peak amplitude is confounded by spikes), firing probability (Fig. 2D),
206 and number of spikes (Fig. 2E) increased in both Het and WT neurons, with no

significant differences between genotypes. Thus, this experiment revealed that activation of the hippocampal microcircuit produces similar responses in CA1 pyramidal neurons despite *Scn1a* haploinsufficiency.

Temporal integration of theta burst activity is unaltered in Scn1a haploinsufficient CA1. While decreased interneuron excitability did not alter the ability of inhibition to gate activation of CA1 pyramidal neurons in response to single SC stimulation, we hypothesized that physiological patterns of activity might cause a breakdown of inhibition and reveal underlying circuit hyperexcitability. We tested this hypothesis by holding neurons in current clamp and stimulating the SC tract with theta bursts (Fig. 3A; 5 bursts, 5 stimuli/burst at 100 Hz, 200 ms intra-burst interval). Theta burst stimulation was repeated at 1x, 3x, and 5x the threshold for evoking reliable responses. The responses of Het neurons were statistically indistinguishable from those of WT neurons. PSP amplitudes for the temporally summed PSPs from each burst (measured as area under the curve with action potentials truncated) were unchanged between genotypes across theta cycles, at each stimulus intensity measured (Fig. 3B; main effect of genotype: $F_{(1,19)} < 0.41$; $p > 0.53$; n = 11 WT; 10 Het). Number of action potentials evoked was also unchanged between genotypes across theta cycles, at each stimulus intensity measured (Fig. 3C). This suggests that even when stimulated with repeated high frequency inputs designed to mimic ongoing physiological activity, GABAergic inhibition was fully functional at controlling CA1 pyramidal neuron activity despite known changes to interneuron physiology caused by *Scn1a* haploinsufficiency.

Reduced feedforward Inhibition onto Het CA1 pyramidal neurons. Our synaptic integration experiments suggested that synaptic inhibition was fully intact, despite well documented changes in interneuron excitability in this model (Favero et al. 2018; Rubinstein et al. 2015; Tai et al. 2014; Yu et al. 2006) Thus, we next sought to determine if changes to inhibitory synaptic physiology could be compensating for changes to excitability. We first measured feedforward synaptic inputs from CA3 to CA1 via stimulation of the SC axons. In these experiments the stimulating electrode was placed relatively distant from the neurons being recorded. In this configuration, GABAergic interneurons were activated by synaptic excitation rather than direct depolarization by the stimulating electrode (Fig. 4A), as evidenced by typical cessation of all synaptic responses after addition of glutamate receptor blockers to the ACSF (Fig. 4C-D). We voltage clamped CA1 pyramidal neurons, using a cesium-based internal solution, alternately at the reversal potential of glutamate (0 mV) and GABA (-70 mV) to isolate excitatory and inhibitory responses. After identifying a threshold stimulus intensity that consistently evoked a minimal response, growth functions were recorded by measuring responses while increasing stimulus current across a broad range of intensities.

For excitatory synaptic responses, statistical comparisons of the amplitude of evoked excitatory postsynaptic currents (EPSC) and the shape of their growth functions revealed no statistical differences between WT and Het neurons (Fig. 4E; main effect of genotype: $F_{(1,16)} = 0.03$; $p = 0.87$, stimulation intensity: $F_{(1.158, 18.53)} = 17.45$; $p < 0.001$, interaction: $F_{(8,128)} = 0.13$; $p = 0.99$; two-way RM-ANOVA). These data show that excitatory synaptic input is normal at this synapse in Het mice with no signs of

compensatory plasticity (e.g., homeostatic scaling). In contrast, comparison of evoked inhibitory postsynaptic current (IPSC) between genotypes revealed a significant change in growth function shape for inhibitory synaptic input as measured by the significant interaction of stimulus intensity and genotype (Fig. 4F; main effect of genotype: $F_{(1,16)}$ = 3.03; p = 0.10, stimulation intensity: $F_{(1.158, 18.53)}$ = 39.11; p < 0.001, interaction: $F_{(8,128)}$ = 4.10; p < 0.001; two-way RM-ANOVA). This result is in line with previous reports of decreased excitability in specific subtypes of hippocampal GABAergic interneurons. It is noteworthy, however, that while the interaction of these two variables that make up the growth function is significant, there was not a significant difference in IPSC amplitude between genotypes either overall or at any individual stimulation intensity (ascertained by post-hoc Sidak's multiple comparisons tests: t < 1.696; p > 0.73). This indicates that despite interneuron intrinsic excitability changes, synaptic inhibition is largely intact in response to single activations of SC axons driving activity through the hippocampal circuit. This is supported by the ratio of excitation to inhibition [EPSC/(EPSC + IPSC)] as a function of stimulus intensity, which revealed no significant changes to this balance even as the circuit was driven by stronger stimuli (Fig. 4G; main effect of genotype: $F_{(1,16)}$ = 1.29; p = 0.22, stimulation intensity: $F_{(1.158, 18.53)}$ = 0.83; p = 0.44, interaction: $F_{(8,128)}$ = 0.11; p = 0.99; two-way RM-ANOVA).

We further examined isolated excitatory and inhibitory synaptic inputs to understand whether the underlying physiology of these synapses was normal or altered after loss of *Scn1a*. Synaptic vesicle release at excitatory synapses, measured by paired pulse ratio (PPR) with an interstimulus interval of 50 ms, was unchanged (Fig 4E_2; p = 0.11; t-test). Similarly, the coefficient of variation (CV) of EPSC amplitude was

relatively low and equivalent across genotypes (Fig. 4E_3; p = 0.33; t-test). These data further indicate that presynaptic physiology of excitatory synapses is grossly normal in Het neurons despite decrements in inhibition and epilepsy caused by *Scn1a* haploinsufficiency.

The CV of IPSC amplitude measured in Het neurons was significantly increased compared with WT (Fig. 4F_2, p = 0.02; t-test). Increased CV is often indicative of a decrease in the number of presynaptic neurons, synapses, or active zones. The PPR for feedforward IPSCs was also significantly increased in Het neurons (Fig. 4F_3; p = 0.02; t-test). It should be noted that PPR for IPSCs in this experiment is confounded by the short-term plasticity of excitatory SC synapses that drive action potential firing in the GABAergic interneurons which then in turn causes synaptic release and IPSCs. Thus, different numbers of interneurons are potentially recruited by the first and second stimulus. As such, this measure of PPR does not reflect an isolated measure of the release properties of inhibitory synapses; direct stimulation of interneurons is necessary to measure short-term facilitation/depression of isolated inhibitory synapses.

To gather more information about the specific properties of excitatory and inhibitory synaptic physiology in Het hippocampi, we isolated and recorded responses to spontaneous release of vesicles in CA1 pyramidal neurons (Fig. 5A). Miniature EPSCs (mEPSCs) were isolated by adding blockers of action potentials (TTX; 1 μM) and synaptic inhibition (gbz; 10 μM) to the ACSF. Comparing Het with WT neurons, there were no differences in mEPSC frequency (Fig. 5C; mEPSC mean frequency: 0.40 ± 0.08 Hz WT; 0.39 ± 0.08 Het; p = 0.97; t-test; Fig. 5D cumulative frequency: p=0.23, K-S test), amplitude (Fig. 5E; mean amplitude: 16.58 ± 1.66 pA WT; 16.90 ± 1.09 Het; p =

299 0.87; t-test), rise time (Fig. 5G; p = 0.72; t-test), or decay kinetics (Fig. 5G; p = 0.62; t-
300 test). As with eEPSCs above, these data indicate normal excitatory synaptic physiology
301 and a lack of compensatory change at glutamatergic synapses.
302 Miniature IPSCs (mIPSCs) were isolated with TTX and glutamatergic blockers
303 (NBQX: 10 μM, APV: 50 μM). mIPSC frequency was significantly reduced in Het
304 neurons compared with WT (Fig. 5C; mIPSC mean frequency: 16.09 ± 2.00 WT; 8.04 ±
305 0.91 Het; p = 0.0007; t-test; Fig. 5E mIPSC cumulative frequency: p<0.0001, K-S test).
306 mIPSC amplitude (Fig. 5E; p = 0.09), rise time (Fig. 5H; p = 0.16), and decay kinetics
307 (Fig. 5H; p = 0.09; t-test) were unchanged between Het and WT neurons. Decreases to
308 mIPSC frequency are often attributable to decreases in vesicle release probability or to
309 the number of inhibitory synapses, which is supported by the increased IPSC CV and
310 PPR reported above.
311
312 *Inhibition onto Scn1a Het CA1 pyramidal neurons is normal when interneurons*
313 *are directly stimulated.* To examine more directly how inhibitory synaptic transmission is
314 altered in Het neurons compared to WT, we performed voltage clamp experiments with
315 the stimulus electrode positioned closer to the recording electrode to directly activate
316 GABAergic interneurons and terminals rather than via excitatory synaptic stimulation of
317 the interneurons. (Fig. 6A). IPSCs were then isolated with glutamate receptor blockers
318 NBQX and APV in the ACSF. As above, IPSC growth functions were recorded by
319 increasing stimulus strength in multiples of the threshold stimulus. Unlike in the indirect
320 stimulation of inhibition experiments, IPSC growth functions showed no deficits in Het
321 neurons (Fig. 6B,C; main effect of genotype: $F_{(1, 20)} = 0.03$; p = 0.86, main effect of stim

intensity: $F_{(1.63, 32.60)} = 15.09$; $p < 0.0001$, interaction: $F_{(8,160)} = 1.05$; $p = 0.40$; two-way RM ANOVA). Also, unlike the direct stimulation experiments, there was no statistical change in IPSC amplitude CV between Het and WT neurons (Fig. 6D; $p = 0.25$; t-test). IPSC PPR was increased in Het neurons compared to WT (Fig. 6E; $p= 0.03$; t-test). No significant changes were revealed in IPSC kinetics (Fig. 6F; rise time: $p= 0.15$; decay tau: $p= 0.12$; Mann-Whitney tests). Overall, these data indicate that despite decreased excitability, *Scn1a* Het interneurons can be recruited by direct stimulation to activate across a broad range of stimulus intensities, resulting in normal levels of synaptic inhibition. Decreased synaptic inhibition growth functions in indirect stimulation experiments (Fig. 4) may thus be a result of decreased synaptic excitation to action potential input/output functions in interneurons. In Het neurons, inhibitory synapses do show an increase in PPR, suggesting a decrease in baseline probability of release that results in a decrease in short-term synaptic depression (which is not caused by changes in kinetics causing temporal summation).

Inhibitory synaptic transmission is stable across frequencies in Het neurons. The data so far reveal that isolated inhibitory synaptic transmission was capable of controlling activity during theta stimulation of SC afferents. We hypothesized that circuit hyperexcitability could be the result of diminished intrinsic excitability in interneurons and inhibitory strength, which would be unmasked when interneurons were driven to fire at higher frequencies and/or for longer durations. To test this hypothesis, we measured isolated synaptic inhibition across theta bursts and during longer stimulus trains of varying frequency. In these experiments excitatory synaptic transmission was

pharmacologically blocked with NBQX and APV and the stimulation electrode placed close enough to directly activate interneurons and GABAergic terminals synaptically linked to the CA1 pyramidal neuron from which we recorded, as in Figure 6A.

Contrary to our hypothesis, hyperpolarization of the membrane was increased in response to theta burst stimulation of synaptic inhibition in Het neurons relative to WT controls (Fig. 7A-C). We adjusted the stimulation intensity to make the initial IPSP of the burst similar in amplitude (~ 2 mV) across cells. Subsequent stimulations resulted in a significantly greater degree of hyperpolarization in Het neurons across the theta cycle (Fig. 7C; main effect of genotype: $F_{(1, 14)} = 6.00$; *p = 0.03, main effect stim number: $F_{(1.60, 22.38)} = 18.51$; $p < 0.0001$, interaction: $F_{(24,336)} = 3.00$; $p < 0.0001$; two-way RM ANOVA). This finding is consistent with the change to PPR illustrated in Figure 6E and is suggested by the decrease in mIPSC frequency in Figure 5C, which indicates that less short-term depression will occur during bursts of activity. The lack of change to IPSC rise and decay kinetics (Fig. 5H), as well as to input resistance and membrane time constant of CA1 pyramidal neurons (Table 1) across genotypes, in combination with these data suggest that increased temporal summation of IPSPs in Het neurons results from a change in pre-synaptic release, rather than postsynaptic receptor or membrane properties.

To further test the durability of inhibition in this system we extended our stimulus paradigm to trains of 20 stimuli, with stimulus frequencies of 10, 50, and 100 Hz (Fig. 7E-G). Synaptic inhibition was robust during these prolonged bursts in both WT and Het neurons. Het neurons exhibited small but statistically significant increases in peak hyperpolarization across the bursts at stimulus frequencies of 10 and 100, but not 50

Hz. These data were recorded in current clamp, and thus do not completely rule out the contribution of activation/deactivation of voltage-gated membrane channels. However, neurons of both genotypes were held at equivalent membrane potentials prior to stimulation and were recorded using the same internal and external solutions, and summed IPSPs are relatively small in magnitude. Taken together, these data indicate that synaptic inhibition onto CA1 pyramidal neurons is not compromised in Het neurons despite well-documented decrements in excitability in major subtypes of hippocampal GABAergic interneurons in *Scn1a* haploinsufficient mouse models.

Discussion

The purpose of these experiments was to gain a deeper understanding of the link between *SCN1A* mutation, loss of function of the voltage-gated sodium channel $Na_v1.1$, and the changes in neural activity and processing that lead to the seizures and cognitive deficits present in *SCN1A*-linked epilepsy disorders. We used an *Scn1a* Het mouse model of Dravet syndrome/epileptic encephalopathy and measured excitatory and inhibitory synaptic transmission and synaptic integration in CA1 hippocampal pyramidal neurons. While we originally hypothesized that hypoexcitability of hippocampal GABAergic interneurons, previously reported at this developmental stage in similar mouse models (Almog et al. 2021; Rubinstein et al. 2015; Yu et al. 2006), would cause network hyperactivity in response to physiologically patterned circuit input and/or compensatory decreases in excitatory synaptic signaling, our data revealed neither of these. Instead, our major findings consist of statistically significant, but relatively subtle, decreased feedforward inhibition, decreased probability of GABAergic synaptic release,

and increased IPSP temporal summation in *Scn1a* Het neurons compared with WT, with a surprising lack of changes to excitatory synaptic physiology and temporal synaptic integration during theta burst activation.

$Na_v1.1$ localizes to somata and dendrites throughout the brain (Gong et al. 1999; Westenbroek et al. 1989), but has been shown to cluster and control action potential generation primarily in GABAergic interneurons (Ogiwara et al. 2007). Gain of function mutations of *SCN1A* are associated with migraine (Dichgans et al. 2005), while loss of function mutations are associated with a broad range of epilepsy syndromes, ranging from the more mild GEFS+ to severe epileptic encephalopathies, including Dravet syndrome (Scheffer and Nabbout 2019). *SCN1A* loss of function animal models, including *Drosophila*, zebrafish, mice, and rats, phenocopy many aspects of Dravet syndrome, like early life pharmacoresistant seizures, wide-ranging neurological deficits, and high levels of early death (Griffin et al. 2018; Schutte et al. 2016). A common thread across models is the cell physiology phenotype of decreased action potential firing of forebrain GABAergic interneurons (Catterall 2018). Information processing in forebrain microcircuits involves finely timed and balanced excitation and inhibition. Thus, we initially hypothesized that decreased inhibition would result in altered synaptic integration in *Scn1a* Het CA1 pyramidal neurons following activation of the hippocampal circuit with physiologically relevant patterned stimuli. However, our findings quite clearly show that both sub- and supra-threshold responses to theta burst protocols were normal in Het pyramidal neurons across a range of stimulus intensities.

While we did not observe the expected changes to synaptic integration of excitation and inhibition, our recordings did reveal changes in GABAergic inhibitory

synaptic transmission in the Het hippocampus. We found a decrease in mIPSC frequency and increases in evoked IPSC PPR and CV when measuring feedforward inhibition, which could be caused by a decrease in the number of inhibitory synaptic inputs and/or a decrease in GABA release probability. While we cannot rule out a decrease in the number of inhibitory synapses, we found that ESPC amplitude and CV normalized when we directly stimulated GABAergic interneurons and terminals, while PPR remained elevated, indicating decreased probability of presynaptic vesicle release at interneuron-CA1 pyramidal neuron synapses. A functional outcome of the decrease in release probability is a reduction in short-term depression, with a net result of increased temporal summation of IPSPs across bursts or trains of synaptic activation. This provides a mechanism by which a reduction in GABA release probability could counteract or even overcome decrements in inhibitory neuron excitability, resulting in normalized synaptic integration during patterns of network activation. While it seems counterintuitive that a decrease in GABAergic release probability could be "compensatory", i.e., protective or corrective in epilepsy, it has the functional effect of increasing the strength of inhibition during physiological patterns of activity. Indeed, GABA release probability is different at synapses onto pyramidal neurons in different brain regions and even across the dorsal-ventral (i.e., septo-temporal) axis of the hippocampus (Milior et al. 2016). Reduced release probability reduces synaptic depression, which can allow for more efficient inhibition during bursts of activity (González et al. 2014). Studies using other mouse models of epilepsy have reported similar reductions in GABA release probability resulting in reduced short-term depression in dentate gyrus granule cells in pilocarpine-induced temporal lobe epilepsy

437 (Faria and Prince 2010; Zhou et al. 2009), and in cortical pyramidal neurons in models
438 of cortical dysplasia (Faria and Prince 2010; Zhou et al. 2009) and post-traumatic
439 epilepsy (Faria and Prince 2010; Zhou et al. 2009). Notably, we cannot directly attribute
440 the mechanism for the changes in synaptic release to *Scn1a* haploinsufficiency (i.e., to
441 a decrease in $Na_v1.1$ channels). Modulation of calcium channel expression has been
442 reported as a mechanism for epilepsy-induced changes in GABA release (Faria et al.
443 2012). Thus, changes to GABAergic synaptic release may be a common compensatory
444 mechanism induced in epilepsy or other disorders to balance excitation and inhibition.
445 Because our data showed that synaptic integration was unchanged in *Scn1a* Het
446 CA1 pyramidal neurons despite interneuron hypoexcitability, we hypothesized that
447 compensatory changes to excitatory synaptic transmission might be occurring in this
448 model. Pyramidal neurons are well-known to have the capacity to change synaptic
449 strength (Turrigiano 2012) and intrinsic excitability (Remy et al. 2010) in response to
450 long-term changes in activity. In mouse models of epilepsy, excitatory synaptic
451 downscaling (Howard et al. 2014; Sun et al. 2013), upscaling (Avramescu and Timofeev
452 2008; Houweling et al. 2005), and decreased intrinsic excitability (Howard et al. 2014)
453 have been reported in CA1 pyramidal neurons. A recent study found increased synaptic
454 strength of glutamatergic cortical inputs to dentate gyrus granule cells in the same
455 *Scn1a* het mouse models used in our study (Mattis et al. 2022). Contrary to our
456 hypothesis, our data did not reveal evidence of compensatory changes to synaptic or
457 intrinsic excitability in *Scn1a* Het CA1 pyramidal cells. This may indicate that altered
458 circuit activity does not reach thresholds for activation of these mechanisms, or that
459 other factors may counterbalance or interfere with the expression of these changes.

While our theta burst synaptic integration experiments suggest that inhibition is functionally strong enough to balance excitation, this does not mean that interneurons in our study were without the well-documented excitability deficits. Our isolated recordings of feedforward IPSCs show clear deficits in response amplitude. When stimulating inhibition onto CA1 pyramidal neurons indirectly, via activation of excitatory SC axons onto interneurons which then release GABA onto the pyramidal neuron, feedforward inhibition was weaker in Het neurons compared to WT. Conversely, when inhibition was stimulated directly, by blocking excitatory transmission and placing the stimulus electrode where interneurons and GABAergic axons and terminals could be directly depolarized, inhibitory strength was equivalent between genotypes. A major difference between these experiments is that indirect stimulation requires synaptic integration, spike initiation at the axon initial segment, and axonal spike propagation by interneurons, each of which could be susceptible to decreased fidelity due to decreased sodium channel activity in Het interneurons. While synaptic transmission and axonal action potential propagation fidelity have not yet been measured directly in *Scn1a* Het models, several reports describe a depolarization of spike threshold in various populations of Het interneurons in ex-vivo slice preparations (Favero et al. 2018; Goff and Goldberg 2019; Rubinstein et al. 2015; Tai et al. 2014), but not in dissociated neurons presumed to be interneurons (Yu et al. 2006). Direct extracellular electrical stimulation of interneurons and GABAergic terminals eliminates synaptic integration and may be strongly suprathreshold, thus masking changes in spike initiation and/or propagation.

Our documentation of synaptic physiology in pyramidal neurons adds further complexity to an already complicated hypothesis of the causal role of inhibitory dysfunction in Dravet syndrome. Interestingly, the intrinsic hypoexcitability of parvalbumin- and somatostatin-expressing interneurons originally discovered in $Na_V1.1$ haploinsufficient mice at age P21 (Tai et al. 2014) normalizes in parvalbumin-positive and hippocampal stratum oriens (largely somatostatin-expressing) interneurons by P35-56 (Almog et al. 2021; Favero et al. 2018). While mortality is at its peak in the earlier period correlating with greatest interneuron dysfunction, seizures and other deficits persist even in Het mice that survive long into adulthood (Han et al. 2012; Kalume et al. 2013; Yu et al. 2006). Our experiments bridged the age range with the most severe mortality (ranging from P21-38). Thus, we sampled from both mice that were likely to die of their epilepsy and those that would have survived long-term. That our data show that inhibitory synaptic transmission remained effective even at relatively high frequencies across extended trains in Het neurons suggests that inhibitory control of neural signaling is intact during most ongoing activity, even when interneurons are hypoexcitable and in mice with the most severe disease. This supports previous work in which *in vivo* recordings of both cortical network activity and identified interneurons were normal in anesthetized and awake Het mice during non-seizure (i.e., inter-ictal) periods in both the severe disease state when interneurons are hypoexcitable (De Stasi et al. 2016; Tran et al. 2020) and at older ages when mortality is low and interneuron excitability has normalized (De Stasi et al. 2016; Tran et al. 2020).

Our findings leave open the questions of where and how the restraints on activity and processing of information by neural circuits break down and result in the seizures

and cognitive deficits present in Dravet syndrome. While inhibitory interneurons exhibit clear hypoexcitability, we found no disruption of inhibition or synaptic integration during "physiological" theta bursts or even extended bursts of stimulation. This shows us that the link between mutation, cellular physiology, and circuit activity is not necessarily direct or intuitive. It may be that our hypotheses and expectations of results are simply incorrect, that our experimental parameters do not cover broad enough ranges, or that our methodologies are not subtle enough to detect nuanced changes. What is clear is that understanding the cell and circuit mechanisms of complex neurological disorders such as Dravet syndrome requires a holistic understanding of direct and indirect changes to the intrinsic and synaptic physiology of many different neuron subtypes and their interactions.

519 **Literature Cited**
520

521 Almog Y, Fadila S, Brusel M, Mavashov A, Anderson K, Rubinstein M. 2021.
522 Developmental alterations in firing properties of hippocampal CA1 inhibitory and
523 excitatory neurons in a mouse model of Dravet syndrome. Neurobiol Dis.
524 148:105209.
525 Avramescu S, Timofeev I. 2008. Synaptic strength modulation after cortical trauma: A
526 role in epileptogenesis. J Neurosci. 28(27):6760-6772.
527 Baraban SC, Dinday MT, Hortopan GA. 2013. Drug screening in Scn1a zebrafish
528 mutant identifies clemizole as a potential dravet syndrome treatment. Nat
529 Commun. 4:2410.
530 Catterall WA. 2018. Dravet syndrome: A sodium channel interneuronopathy. Curr Opin
531 Physiol. 2:42-50.
532 Catterall WA, Kalume F, Oakley JC. 2010. $Na_v1.1$ channels and epilepsy. J Physiol.
533 588(Pt 11):1849-1859.
534 Claes L, Del-Favero J, Ceulemans B, Lagae L, Van Broeckhoven C, De Jonghe P.
535 2001. De novo mutations in the sodium-channel gene SCN1A cause severe
536 myoclonic epilepsy of infancy. Am J Hum Genet. 68(6):1327-1332.
537 De Stasi AM, Farisello P, Marcon I, Cavallari S, Forli A, Vecchia D, Losi G, Mantegazza
538 M, Panzeri S, Carmignoto G et al. 2016. Unaltered network activity and
539 interneuronal firing during spontaneous cortical dynamics in vivo in a mouse
540 model of severe myoclonic epilepsy of infancy. Cereb Cortex. 26(4):1778-1794.
541 Dichgans M, Freilinger T, Eckstein G, Babini E, Lorenz-Depiereux B, Biskup S, Ferrari
542 MD, Herzog J, van den Maagdenberg AM, Pusch M et al. 2005. Mutation in the

neuronal voltage-gated sodium channel SCN1A in familial hemiplegic migraine. Lancet. 366(9483):371-377.

Dougherty KA, Islam T, Johnston D. 2012. Intrinsic excitability of CA1 pyramidal neurones from the rat dorsal and ventral hippocampus. J Physiol. 590(22):5707-5722.

Dravet C. 2011. The core Dravet syndrome phenotype. Epilepsia. 52 Suppl 2:3-9.

Dyment DA, Schock SC, Deloughery K, Tran MH, Ure K, Nutter LMJ, Creighton A, Yuan J, Banderali U, Comas T et al. 2020. Electrophysiological alterations of pyramidal cells and interneurons of the CA1 region of the hippocampus in a novel mouse model of Dravet syndrome. Genetics. 215(4):1055-1066.

Escayg A, Goldin AL. 2010. Sodium channel SCN1A and epilepsy: Mutations and mechanisms. Epilepsia. 51(9):1650-1658.

Faria LC, Parada I, Prince DA. 2012. Interneuronal calcium channel abnormalities in posttraumatic epileptogenic neocortex. Neurobiol Dis. 45(2):821-828.

Faria LC, Prince DA. 2010. Presynaptic inhibitory terminals are functionally abnormal in a rat model of posttraumatic epilepsy. J Neurophysiol. 104(1):280-290.

Favero M, Sotuyo NP, Lopez E, Kearney JA, Goldberg EM. 2018. A transient developmental window of fast-spiking interneuron dysfunction in a mouse model of Dravet syndrome. J Neurosci. 38(36):7912-7927.

Goff KM, Goldberg EM. 2019. Vasoactive intestinal peptide-expressing interneurons are impaired in a mouse model of Dravet syndrome. Elife. 8.

Gong B, Rhodes KJ, Bekele-Arcuri Z, Trimmer JS. 1999. Type I and type II Na(+) channel alpha-subunit polypeptides exhibit distinct spatial and temporal

patterning, and association with auxiliary subunits in rat brain. J Comp Neurol. 412(2):342-352.

González JC, Lignani G, Maroto M, Baldelli P, Hernández-Guijo JM. 2014. Presynaptic muscarinic receptors reduce synaptic depression and facilitate its recovery at hippocampal gabaergic synapses. Cereb Cortex. 24(7):1818-1831.

Griffin A, Hamling KR, Hong S, Anvar M, Lee LP, Baraban SC. 2018. Preclinical animal models for Dravet syndrome: Seizure phenotypes, comorbidities and drug screening. Front Pharmacol. 9:573.

Han S, Tai C, Westenbroek RE, Yu FH, Cheah CS, Potter GB, Rubenstein JL, Scheuer T, de la Iglesia HO, Catterall WA. 2012. Autistic-like behaviour in Scn1a+/- mice and rescue by enhanced gaba-mediated neurotransmission. Nature. 489(7416):385-390.

Hedrich UB, Liautard C, Kirschenbaum D, Pofahl M, Lavigne J, Liu Y, Theiss S, Slotta J, Escayg A, Dihné M et al. 2014. Impaired action potential initiation in gabaergic interneurons causes hyperexcitable networks in an epileptic mouse model carrying a human Na(v)1.1 mutation. J Neurosci. 34(45):14874-14889.

Houweling AR, Bazhenov M, Timofeev I, Steriade M, Sejnowski TJ. 2005. Homeostatic synaptic plasticity can explain post-traumatic epileptogenesis in chronically isolated neocortex. Cereb Cortex. 15(6):834-845.

Howard MA, Rubenstein JL, Baraban SC. 2014. Bidirectional homeostatic plasticity induced by interneuron cell death and transplantation in vivo. Proc Natl Acad Sci U S A. 111(1):492-497.

588 Kalume F, Westenbroek RE, Cheah CS, Yu FH, Oakley JC, Scheuer T, Catterall WA.
589 2013. Sudden unexpected death in a mouse model of Dravet syndrome. J Clin
590 Invest. 123(4):1798-1808.
591 Malik R, Dougherty KA, Parikh K, Byrne C, Johnston D. 2016. Mapping the
592 electrophysiological and morphological properties of CA1 pyramidal neurons
593 along the longitudinal hippocampal axis. Hippocampus. 26(3):341-361.
594 Marini C, Scheffer IE, Nabbout R, Suls A, De Jonghe P, Zara F, Guerrini R. 2011. The
595 genetics of Dravet syndrome. Epilepsia. 52 Suppl 2:24-29.
596 Mashimo T, Ohmori I, Ouchida M, Ohno Y, Tsurumi T, Miki T, Wakamori M, Ishihara S,
597 Yoshida T, Takizawa A et al. 2010. A missense mutation of the gene encoding
598 voltage-dependent sodium channel ($Na_v1.1$) confers susceptibility to febrile
599 seizures in rats. J Neurosci. 30(16):5744-5753.
600 Mattis J, Somarowthu A, Goff KM, Jiang E, Yom J, Sotuyo N, Mcgarry LM, Feng H,
601 Kaneko K, Goldberg EM. 2022. Corticohippocampal circuit dysfunction in a
602 mouse model of Dravet syndrome. Elife. 11.
603 Milior G, Di Castro MA, Sciarria LP, Garofalo S, Branchi I, Ragozzino D, Limatola C,
604 Maggi L. 2016. Electrophysiological properties of CA1 pyramidal neurons along
605 the longitudinal axis of the mouse hippocampus. Sci Rep. 6:38242.
606 Miller AR, Hawkins NA, McCollom CE, Kearney JA. 2014. Mapping genetic modifiers of
607 survival in a mouse model of Dravet syndrome. Genes Brain Behav. 13(2):163-
608 172.

609 Mistry AM, Thompson CH, Miller AR, Vanoye CG, George AL, Kearney JA. 2014.
610 Strain- and age-dependent hippocampal neuron sodium currents correlate with
611 epilepsy severity in Dravet syndrome mice. Neurobiol Dis. 65:1-11.
612 Ogiwara I, Miyamoto H, Morita N, Atapour N, Mazaki E, Inoue I, Takeuchi T, Itohara S,
613 Yanagawa Y, Obata K et al. 2007. Nav1.1 localizes to axons of parvalbumin-
614 positive inhibitory interneurons: A circuit basis for epileptic seizures in mice
615 carrying an Scn1a gene mutation. J Neurosci. 27(22):5903-5914.
616 Poolos NP, Jones TD. 2004. Patch-clamp recording from neuronal dendrites. Curr
617 Protoc Neurosci. Chapter 6:Unit 6.19.
618 Remy S, Beck H, Yaari Y. 2010. Plasticity of voltage-gated ion channels in pyramidal
619 cell dendrites. Curr Opin Neurobiol. 20(4):503-509.
620 Rubinstein M, Westenbroek RE, Yu FH, Jones CJ, Scheuer T, Catterall WA. 2015.
621 Genetic background modulates impaired excitability of inhibitory neurons in a
622 mouse model of Dravet syndrome. Neurobiol Dis. 73:106-117.
623 Scheffer IE, Nabbout R. 2019. SCN1A-related phenotypes: Epilepsy and beyond.
624 Epilepsia. 60 Suppl 3:S17-S24.
625 Schutte SS, Schutte RJ, Barragan EV, O'Dowd DK. 2016. Model systems for studying
626 cellular mechanisms of Scn1a-related epilepsy. J Neurophysiol. 115(4):1755-
627 1766.
628 Stuart GJ, Spruston N. 2015. Dendritic integration: 60 years of progress. Nat Neurosci.
629 18(12):1713-1721.
630 Sun H, Kosaras B, Klein PM, Jensen FE. 2013. Mammalian target of rapamycin
631 complex 1 activation negatively regulates polo-like kinase 2-mediated

homeostatic compensation following neonatal seizures. Proc Natl Acad Sci U S A. 110(13):5199-5204.

Sun L, Gilligan J, Staber C, Schutte RJ, Nguyen V, O'Dowd DK, Reenan R. 2012. A knock-in model of human epilepsy in Drosophila reveals a novel cellular mechanism associated with heat-induced seizure. J Neurosci. 32(41):14145-14155.

Tai C, Abe Y, Westenbroek RE, Scheuer T, Catterall WA. 2014. Impaired excitability of somatostatin- and parvalbumin-expressing cortical interneurons in a mouse model of Dravet syndrome. Proc Natl Acad Sci U S A. 111(30):E3139-3148.

Tran CH, Vaiana M, Nakuci J, Somarowthu A, Goff KM, Goldstein N, Murthy P, Muldoon SF, Goldberg EM. 2020. Interneuron desynchronization precedes seizures in a mouse model of Dravet syndrome. J Neurosci. 40(13):2764-2775.

Turrigiano G. 2012. Homeostatic synaptic plasticity: Local and global mechanisms for stabilizing neuronal function. Cold Spring Harb Perspect Biol. 4(1):a005736.

Westenbroek RE, Merrick DK, Catterall WA. 1989. Differential subcellular localization of the RI and RII Na+ channel subtypes in central neurons. Neuron. 3(6):695-704.

Yu FH, Mantegazza M, Westenbroek RE, Robbins CA, Kalume F, Burton KA, Spain WJ, McKnight GS, Scheuer T, Catterall WA. 2006. Reduced sodium current in gabaergic interneurons in a mouse model of severe myoclonic epilepsy in infancy. Nat Neurosci. 9(9):1142-1149.

Zhou FW, Chen HX, Roper SN. 2009. Balance of inhibitory and excitatory synaptic activity is altered in fast-spiking interneurons in experimental cortical dysplasia. J Neurophysiol. 102(4):2514-2525.

Figure Legends

Figure 1. Verification of reported *Scn1a+/-* phenotypes. A) Survival plot of *Scn1a +/-* (blue; n = 25) and *Scn1a +/+* wild type litter mates (WT; gray; n = 30) from 7 litters, plotted as probability of survival per day. *** $p < 0.001$, χ^2 test. All electrophysiology experiments were done during the period shaded in orange (P21-38). **B)** Example whole-cell recordings of neuron membrane potential to depolarizing current steps (100, 200 and 300 pA steps). C) Spike number plotted as a function of current step size (main effect of current step: $F_{(12, 180)} = 62.73$; $p < 0.0001$; genotype: $F_{(1, 15)} = 0.03$; $p = 0.87$; interaction: $F_{(12, 180)} = 0.16$; $p = 0.99$).

Figure 2. Similar postsynaptic potentials in CA1 pyramidal neurons from WT and *Scn1a+/-* mice. A) Example PSPs recorded in CA1 pyramidal cells from *Scn1a+/+* (WT; gray) and *Scn1a+/-* (Het; blue) mice in response to single stimulations of Schaffer collateral axons at 1, 3, and 5x the minimal stim intensity in ACSF (top) and 3x the minimal stim in 10 μM gabazine (gbz, bottom). **B)** The peak amplitude across a range of stim intensities is similar between genotypes (main effect of genotype: $F_{(1,19)} = 0.62$; $p = 0.44$, main effect of stim intensity: $F_{(1.57, 29.83)} = 51.18$; $p < 0.0001$, interaction: $F_{(8,152)} = 1.11$; $p = 0.36$; two-way RM ANOVA; n = (cells/mice)). **C)** Firing probability across stim intensities is similar between genotypes (main effect of genotype: $F_{(1,38)} = 0.09$; $p = 0.77$; main effect of stim intensity: $F_{(2.68, 101.7)} = 7.09$; $p < 0.001$; three-way RM ANOVA), and is similarly increased by gbz application in both genotypes (main effect of drug:

678 $F_{(1,38)}$ = 21.98; p < 0.0001; genotype x drug: $F_{(1,38)}$ = 0.76; p = 0.39) **D)** Area under the
679 curve, with spikes truncated, across stim intensities is similar between genotypes (main
680 effect of genotype: $F_{(1,38)}$ = 0.96; p = 0.33; main effect of stim intensity: $F_{(2.68, 101.7)}$ =
681 19.23; p < 0.0001, main effect of drug: $F_{(1,38)}$ = 24.21; p < 0.0001; genotype x drug:
682 $F_{(1,38)}$ = 1.11, p = 0.30; three-way RM ANOVA). **E)** The number of spikes fired in gbz
683 was also similar between genotypes (main effect of genotype: $F_{(1,19)}$ = 0.01; p = 0.90,
684 main effect of stim intensity: $F_{(1.57, 29.83)}$ = 6.96; p < 0.01, interaction: $F_{(8,152)}$ = 0.69; p =
685 0.70; two-way RM ANOVA).
686
687 **Figure 3. Normal temporal synaptic integration in *Scn1a*+/- neurons. A)** Example
688 PSPs recorded in CA1 pyramidal cells from *Scn1a*+/+ (top, gray) and *Scn1a*+/- (bottom,
689 blue) mice in response to theta burst stimulation (hash marks below) of Schaffer
690 collateral axons at 1, 3, and 5x the minimal stim intensity with no synaptic blockers. **B)**
691 No change in amplitude of PSPs, measured as area under the curve, between
692 genotypes (main effect of genotype: $F_{(1,19)}$ < 0.41; p > 0.53; n = (cells/mice)). **C)** No
693 difference in number of action potentials fired in response to theta stimulation between
694 genotypes (main effect of genotype: $F_{(1, 19)}$ = 0.06; p = 0.81, main effect of stim intensity:
695 $F_{(1.04, 19.82)}$ = 4.40; p = 0.048, interaction: $F_{(2,38)}$ = 0.19; p = 0.83; two-way RM ANOVA).
696
697 **Figure 4. Reduced feedforward inhibitory input to *Scn1a*+/- CA1 pyramidal**
698 **neurons. A)** Experimental design: We performed whole-cell voltage-clamp recordings
699 of CA1 pyramidal cells. Schaffer collateral axons were stimulated upstream from the
700 CA1 pyramidal neuron, which directly release glutamate onto the CA1 pyramidal neuron

to generate an excitatory postsynaptic current (EPSC), and onto inhibitory interneurons that then provide GABAergic inhibitory postsynaptic currents (IPSCs) to the pyramidal cells. **B)** Example traces of excitatory (recorded at E_{gaba} = -70 mV) and inhibitory (recorded at $E_{glutamate}$ = 0 mV) postsynaptic currents in WT (left, gray) and *Scn1a*$^{+/-}$ (right, blue) neurons evoked at the minimal stimulation intensity required to evoke an EPSC (1x), 3x, and 5x the minimal intensity. **C)** Example traces of IPSCs recorded in ACSF (black), in the presence of glutamate blockers (10 μM NBQX, 50 μM D-AP5, red) and in the presence of glutamate blockers + gabazine (10 μM, gray), demonstrating that the majority of the GABAergic input using this paradigm was feedforward inhibition. **D)** 79.4% in WTs; 86.7% in *Scn1a*$^{+/-}$; p = 0.38, t-test. **E_1)** Peak amplitude of ESPCs by stimulation intensity is similar between genotypes (main effect of genotype: $F_{(1,16)}$ = 0.03; p = 0.87, main effect of stimulation intensity: $F_{(1.158, 18.53)}$ = 17.45; p < 0.001, interaction: $F_{(8,128)}$ = 0.13; p = 0.99; two-way ANOVA; n = (cells/mice)). **E_2)** The coefficient of variation (CV) measured using 50 stimulations at 2.5x the minimal stim intensity (p = 0.33; n=11 WT and n=11 *Scn1a*$^{+/-}$) and **E_3)** and paired-pulse ratio (PPR)of EPSCs (p = 0.11; n = 24 WT and n = 31 *Scn1a*$^{+/-}$; t-test) are not different between WT and *Scn1a*$^{+/-}$ neurons. **F_1)** The IPSC growth curve is reduced in *Scn1a*+/- neurons compared to WT (main effect of genotype: $F_{(1,16)}$ = 3.03; p = 0.10, main effect of stimulation intensity: $F_{(1.158, 18.53)}$ = 39.11; p < 0.001, interaction: $F_{(8,128)}$ = 4.10; p < 0.001). **F_2)** The CV of IPSCs is increased in *Scn1a*$^{+/-}$ neurons (*p = 0.02; n=11 WT and n=11 *Scn1a*$^{+/-}$), and **F_3)** PPR is increased (*p = 0.02; n=26 WT and n=31 *Scn1a*$^{+/-}$). **G)** Excitatory to inhibitory ratio, measured as the [area of the EPSC/(area of EPSC + area of IPSC)] was similar in WT and *Scn1a*$^{+/-}$ neurons across stim intensities (main effect of

724 genotype: $F_{(1,16)} = 1.29$; $p = 0.22$, stimulation intensity: $F_{(1.158, 18.53)} = 0.83$; $p = 0.44$,
725 interaction: $F_{(8,128)} = 0.11$; $p = 0.99$; two-way ANOVA).
726
727 **Figure 5. Reduced miniature IPSC frequency to *Scn1a+/-* CA1 pyramidal neurons.**
728 **A)** Example raw traces of mEPSCs, recorded in gabazine (10 μM) and 1 μM TTX (left)
729 and averages (right). **B)** Example mIPSCs recorded in glutamate blockers (10 μM
730 NBQX, 50 μM D-AP5). **C)** The frequency of mEPSCs in unchanged, but mIPSCs are
731 reduced in *Scn1a*$^{+/-}$ neurons (*** $p < 0.001$; t-test; N = 10 cells from 4 mice WT; n = 13
732 cells from 6 mice *Scn1a*$^{+/-}$). **D)** The lack of change in mEPSC frequency between WT
733 and *Scn1a*$^{+/-}$ neurons is demonstrated in the similar cumulative frequency of inter-event
734 intervals plot. **E)** The cumulative frequency plot of mIPSCs is shifted to the right for
735 *Scn1a*$^{+/-}$ neurons (K-S test). **F)** The amplitude and **G-H)** kinetics of miniature EPSCs and
736 IPSCs are similar between genotypes ($p > 0.05$; t-test).
737
738 **Figure 6. Direct activation of inhibitory interneurons reveals normal amplitude but**
739 **more facilitating GABAergic responses in CA1 pyramidal neurons. A)**
740 Experimental design: We stimulated near the recorded CA1 pyramidal cell (PC) in the
741 presence of glutamatergic blockers (10 μM NBQX, 50 μM D-AP5) to directly activate
742 local GABAergic interneurons (IN) and axons. **B)** Example traces of IPSCs from WT
743 (left, gray) and *Scn1a*$^{+/-}$ (right, blue) neurons evoked at the minimal stimulation intensity
744 required to evoke an EPSC (1x), 3x, and 5x the minimal intensity (top). Bottom: overlaid
745 paired-pulse stimulation (50 ms isi) traces recorded at 2.5x the minimal stim intensity,
746 normalized to the peak of the first stimulation. **C) I**PSC growth functions showed no

deficits in *Scn1a*$^{+/-}$ neurons (main effect of genotype: $F_{(1, 20)} = 0.03$; $p = 0.86$, main effect of stim intensity: $F_{(1.63, 32.60)} = 15.09$; $p < 0.0001$, interaction: $F_{(8,160)} = 1.05$; $p = 0.40$; two-way RM ANOVA). **D)** No difference in coefficient of variation (CV) of IPSCs measured using 50 stimulations at 2.5x the minimal stim intensity ($p = 0.25$, t-test). **E)** IPSC paired-pulse ratio (PPR) is increased in *Scn1a*$^{+/-}$ neurons (*$p = 0.03$; t-test). **F)** No difference in IPSC kinetics between genotypes (rise: $p = 0.15$; decay: $p = 0.12$; Mann-Whitney tests).

Figure 7. IPSPs are less depressing in *Scn1a+/-* animals and provide increased inhibition at higher frequency stimulation. A) Example traces of IPSPs in response to theta-burst stimulation from WT (top, gray) and Het (bottom, blue) neurons. **B)** Overlaid traces of the first burst from the theta burst paradigm demonstrating that responses in WT neurons were much more depressing than those from *Scn1a*$^{+/-}$ neurons. Stim intensity was normalized to generate the same amplitude (~2 mV) for the first IPSP across cells. **C)** IPSP maximum hyperpolarization for each stimulation in the theta burst paradigm in increased in *Scn1a*$^{+/-}$ neurons (main effect of genotype: $F_{(1, 14)} = 6.00$; *$p = 0.03$, main effect stim number: $F_{(1.60, 22.38)} = 18.51$; $p < 0.0001$, interaction: $F_{(24,336)} = 3.00$; $p < 0.0001$; two-way RM ANOVA; n = (cells/mice)). **D)** PPR of IPSPs (amplitude of 2nd IPSP/1st IPSP) across a range of stim intensities showing that IPSPs are less depressing in *Scn1a*$^{+/-}$ neurons at higher frequencies (main effect of genotype: $F_{(1, 9)} = 1.18$; $p = 0.31$; main effect frequency: $F_{(1.69, 15.17)} = 2.03$; $p = 0.17$, interaction: $F_{(4, 36)} = 2.29$; $p < 0.08$; two-way RM ANOVA; **$p < 0.01$ Sidak's multiple comparisons test). **E)** IPSP peak hyperpolarization in response to 20 stimulations at 10 Hz, (main

effect of genotype: $F_{(1, 280)} = 8.86$; **p = 0.003, stim number: $F_{(19, 280)} = 0.02$; p > 0.99, interaction: $F_{(19,280)} = 0.01$; p > 0.99; two-way RM ANOVA), **F)** 50 Hz (main effect of genotype: $F_{(1, 280)} = 0.41$; p = 0.52, stim number: $F_{(19, 280)} = 0.18$; p > 0.99, interaction: $F_{(19,280)} = 0.02$; p > 0.99)and **G)** 100 Hz (main effect of genotype: $F_{(1, 280)} = 7.49$; **p = 0.006, stim number: $F_{(19, 280)} = 0.58$; p = 0.92, interaction: $F_{(19,280)} = 0.03$; p > 0.99)

777

778 TABLE 1: Intrinsic electrophysiological properties of CA1 pyramidal neurons

	WT (n=7 cells from 5 mice)	*Het* (n=10 cells from 7 mice)	p value (unpaired t-test)
Resting membrane potential (mV)	-60.59 ± 1.83	-58.40 ± 1.61	0.385
Input resistance (MΩ)	136.60 ± 16.90	118.00 ± 10.34	0.335
Membrane time constant (ms)	17.19 ± 2.12	12.64 ± 6.06	0.138
Capacitance (pF)	132.00 ± 13.6	112.10 ± 18.00	0.428
Voltage sag (mV)	5.81 ± 0.52	6.72 ± 0.44	0.190
Rheobase (pA)	153.60 ± 24.7	140.00 ± 13.50	0.611
Voltage threshold (mV)	-39.22 ± 1.70	-38.25 ± 1.05	0.617
1st spike rise time (µs)	269.40 ± 21.21	255.50 ± 22.68	0.674
1st spike half width (ms)	1.49 ± 0.12	1.36 ± 0.09	0.375

779

780

Figure 1

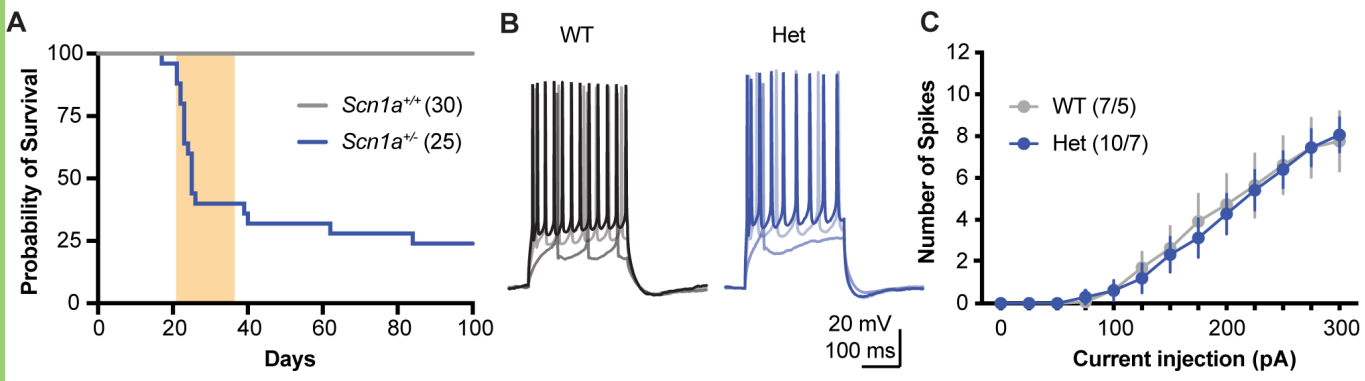

Figure 2

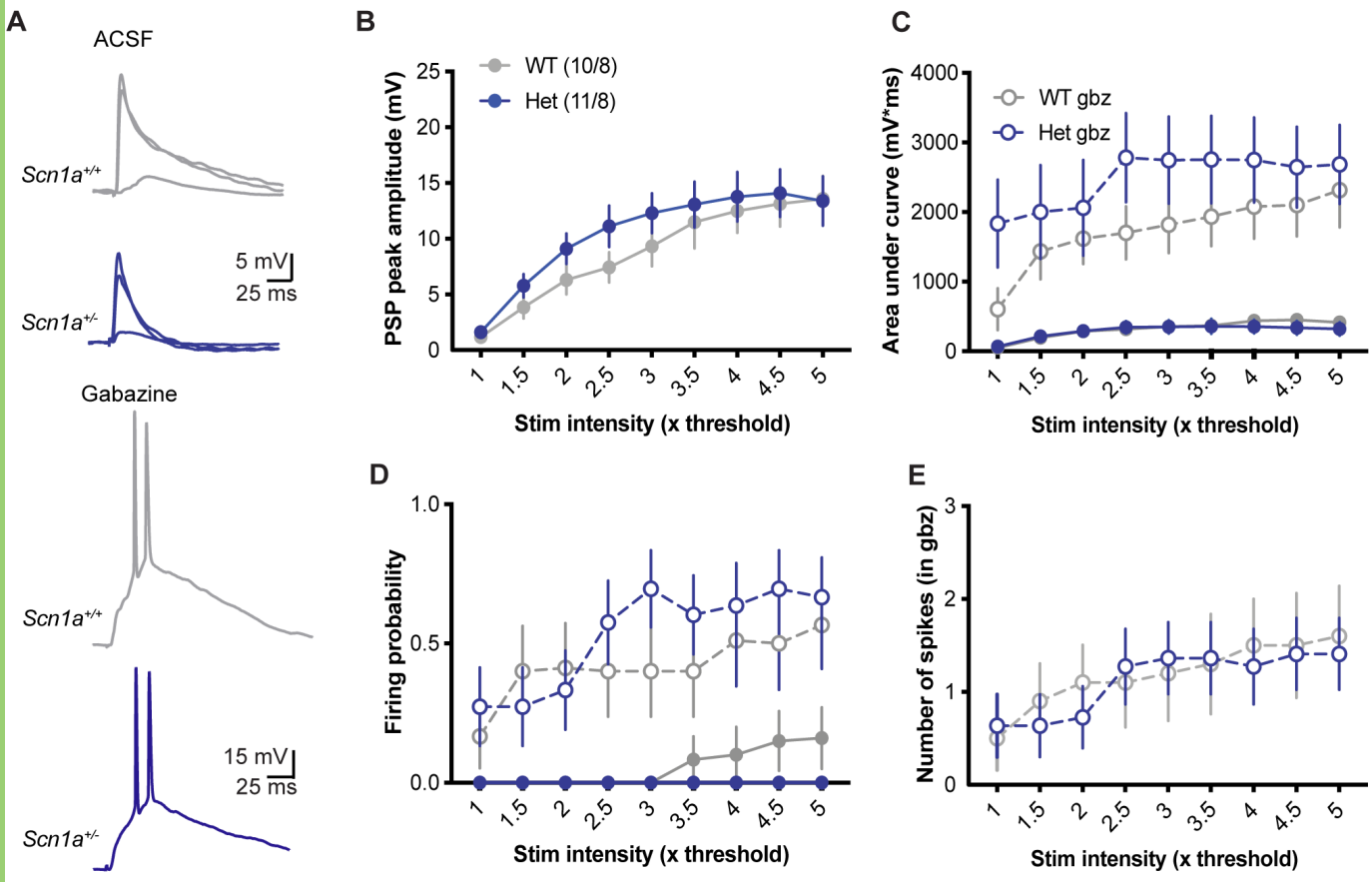

Figure 3

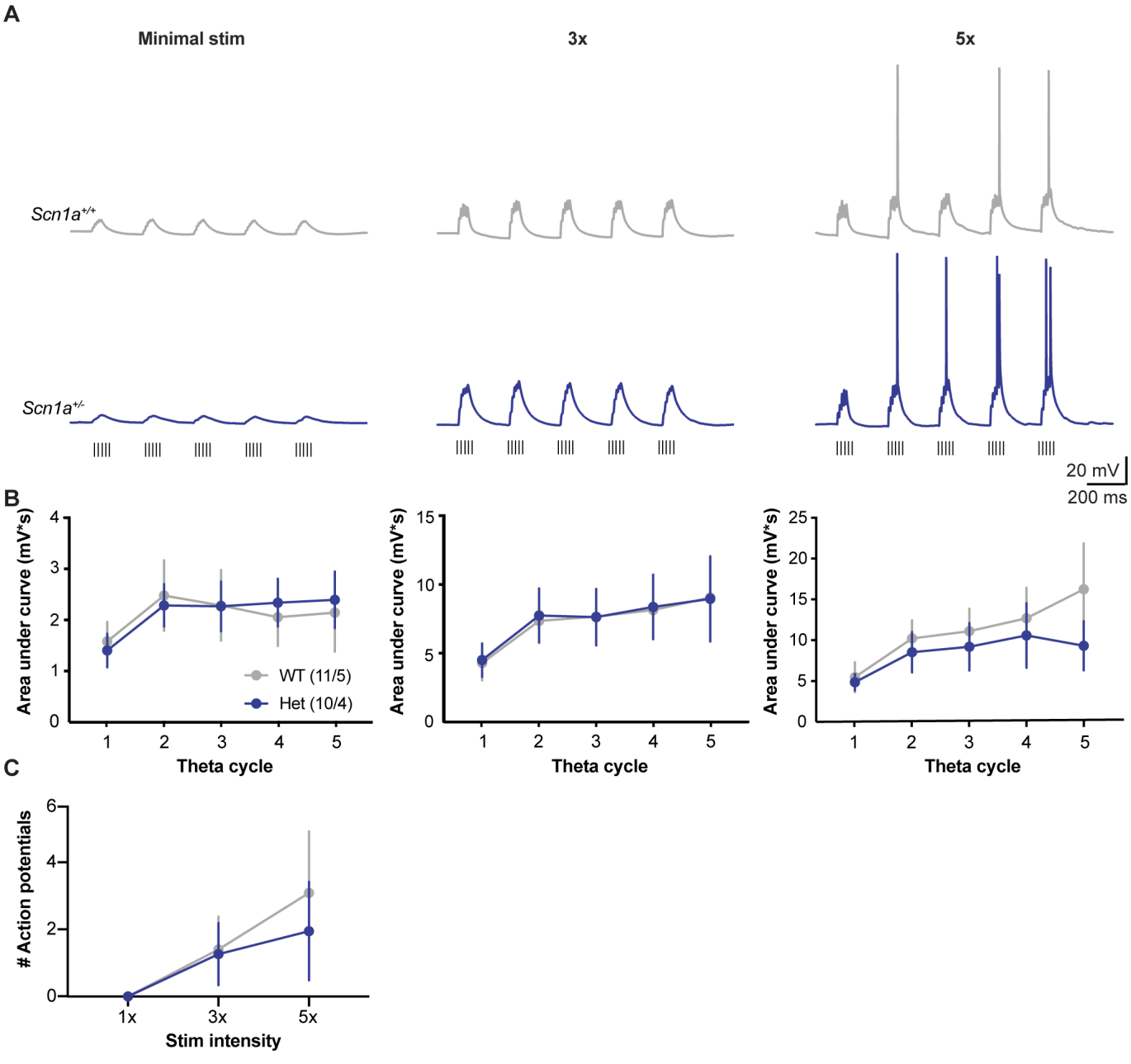

Figure 4

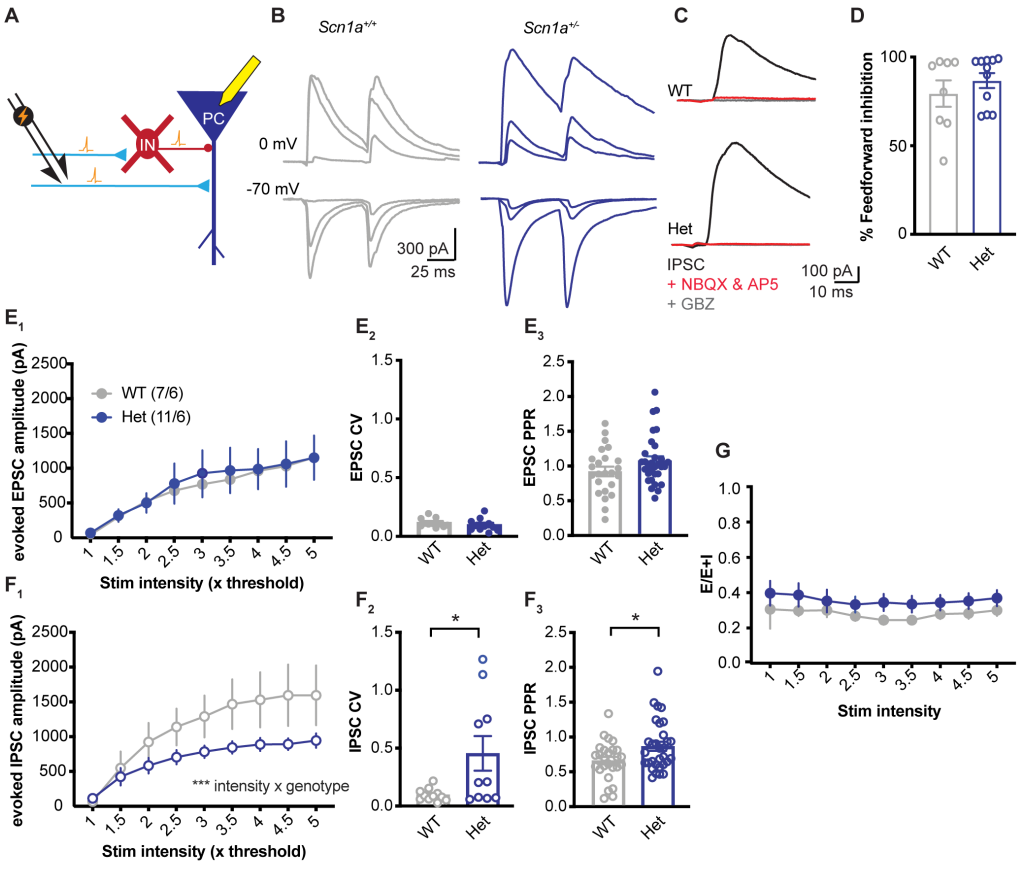

Figure 5

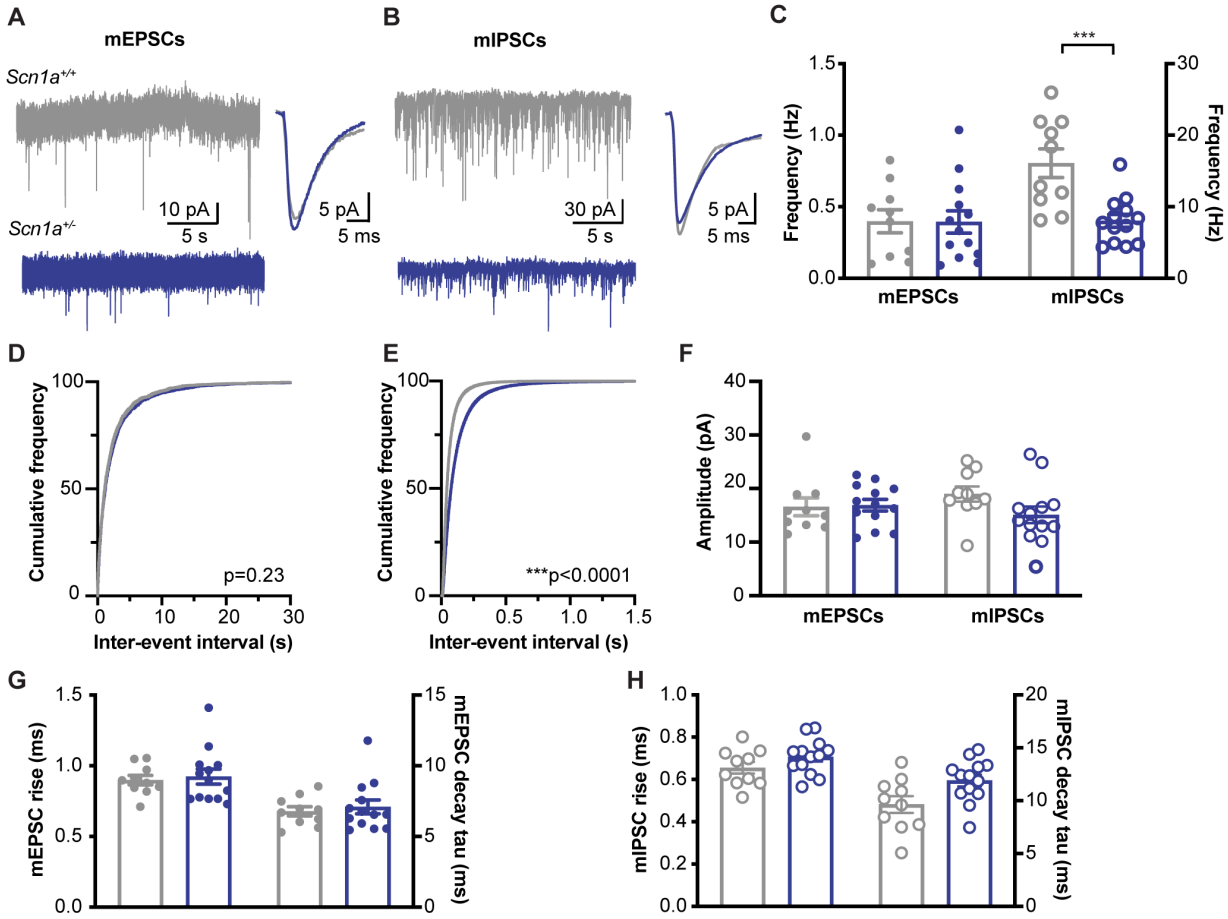

Figure 6

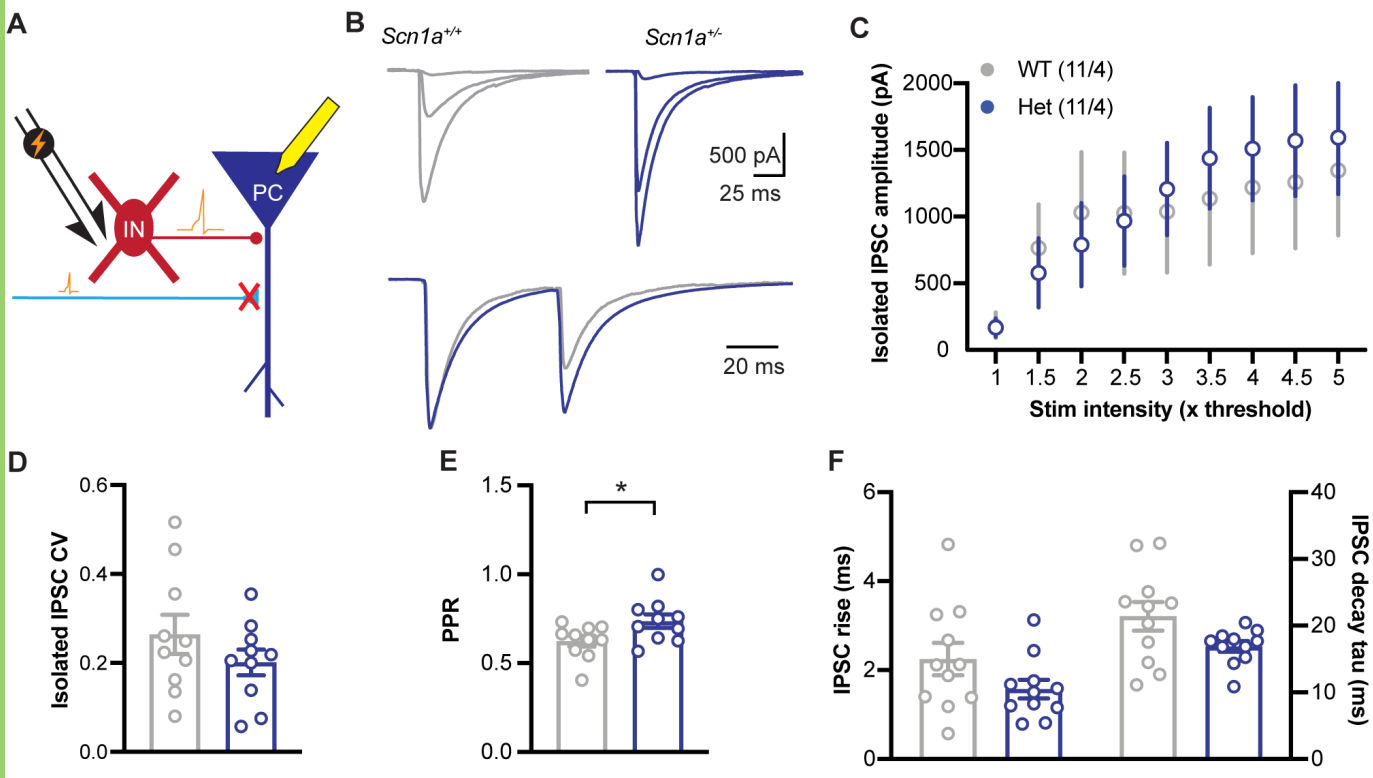

Figure 7